# Effective viscosity of two-dimensional suspensions: Confinement effects

Vincent Doyeux,[1] Stephane Priem,[1] Levan Jibuti,[2] Alexander Farutin,[1]
Mourad Ismail,[1] and Philippe Peyla[1,*]
[1]*Laboratoire Interdisciplinaire de Physique, Universitité Grenoble Alpes, CNRS, 38000 Grenoble, France*
[2]*Theoretische Physik I, University of Bayreuth, 95440 Bayreuth, Germany*
(Received 16 March 2016; published 24 August 2016)

We study the rheology of a sheared two-dimensional (2D) suspension of non-Brownian disks in the presence of walls. Although it is of course possible today with modern computers and powerful algorithms to perform direct numerical simulations that fully account for multiparticle 3D interactions in the presence of walls, the analysis of the simple case of a 2D suspension provides valuable insights and helps in the understanding of 3D results. Due to the direct visualization of the whole 2D flow (the shear plane), we are able to give a clear interpretation of the full hydrodynamics of semidilute confined suspensions. For instance, we examine the role of disk-wall and disk-disk interactions to determine the dissipation of confined sheared suspensions whose effective viscosity depends on the area fraction $\phi$ of the disks as $\eta_{\text{eff}} = \eta_0[1 + [\eta]\phi + \beta\phi^2 + O(\phi^3)]$. We provide numerical estimates of $[\eta]$ and $\beta$ for a wide range of confinements. As a benchmark for our simulations, we compare the numerical results obtained for $[\eta]$ and $\beta$ for very weak confinements with analytical values $[\eta]_\infty$ and $\beta_\infty$ obtained for an infinite fluid. If the value $[\eta]_\infty = 2$ is well known in the literature, much less is published on the value of $\beta$. Here we analytically calculate with very high precision $\beta_\infty = 3.6$. We also reexamine the 3D case in the light of our 2D results.

DOI: 10.1103/PhysRevFluids.1.043301

## I. INTRODUCTION

Understanding the macroscopic transport and flow behavior of particles or fibers suspended in a fluid medium is important to several industries that handle, for example, slurries, ceramics, colloids, or polymers. Usually negligible or small Reynolds numbers Re are considered since this situation is more relevant regarding the high viscosity of suspensions. An external flow moves micron-scale objects that are strongly coupled to each other by hydrodynamic interactions (HIs) [1–3]. Two-dimensional (2D) simulations represent an efficient and convenient tool for understanding some phenomena arising in hydrodynamics of suspensions. For example, 2D simulations have been used to study flow past 2D single bodies of arbitrary cross-sectional shape [4] or around rotating circular cylinder in a shear flow at low Reynolds number [5]. Two-dimensional simulations have also been used to study multiparticle systems such as diffusing proteins in biological membranes [6], suspensions of red blood cells [7], vesicles [8] or capsules [9,10]. Two-dimensional simulations are much less time and memory consuming than 3D ones. In two dimensions, very simple visualizations of the entire flow are easy and render clear insight into 3D problems that are sometimes quite difficult to understand. Several publications have been dedicated to 2D suspensions and their rheology from dilute to large volume fractions [6,11,12]. In this paper we are interested in the rheology of confined suspensions. Low-Re flows of suspensions of neutrally buoyant particles sheared or confined between two walls [13–21] or transported through channels [7,22–25] of width comparable to the particle dimension are very important because of their occurrence in many experimental, biological, and technological systems including blood flow in capillaries or in confined flows [7], and also flows in porous media [26] or in microfluidic devices [27].

*philippe.peyla@univ-grenoble-alpes.fr

 

It was shown [19] that the contribution of 3D hydrodynamic interactions in the semidilute regime to the effective viscosity becomes negative for very confined hard and non-Brownian spheres. This was further confirmed by another theoretical approach [21] and by experiments [20]. This effect survives for finite Re (Re $\approx 5$) [28]. In this work we observe the same phenomenon for the 2D case (with Re $= 0$) and we can give a simple interpretation of the variation of the effective viscosity with confinement by examining the dissipation density and the fluid flow around particles. Our 2D simulations can clarify points that were still unclear such as the contribution of the HI to the effective viscosity in high confinement cases. We focus our study on disk-wall HIs in the dilute case and disk-disk HIs in the presence of walls for semidilute 2D suspensions.

The volume fraction $\phi$ is usually defined as the total volume of $N$ spherical particles of radius $a$ divided by the whole volume $V$ of the suspension: $\phi_{3D} = N\frac{4}{3}\pi a^3/V$. Here, in two dimensions, we define an area fraction $\phi_{2D} = N\pi a^2/S$, where $S$ represents the total area of the suspension. For convenience, in the rest of the paper we drop the 2D subscript and we refer to the volume fraction even in two dimensions. When we refer to the 3D case, no ambiguity remains. Whatever the dimension, the effective viscosity of the whole suspension depends nonlinearly on $\phi$ and can be expressed as a virial expansion [3] in the semidilute case where pair interactions start to operate between particles:

$$\eta_{\text{eff}} = \eta_0\{1 + [\eta]\phi + \beta\phi^2 + O(\phi^3)\}, \tag{1}$$

where $[\eta]$ is the Einstein viscosity, representing the contribution of each particle to $\eta_{\text{eff}}$. The coefficient $\beta$ is the contribution of HIs between pairs of particles to $\eta_{\text{eff}}$. Previous studies [6,11,12] on rheology of 2D suspensions have generally focused on the behavior of $\eta_{\text{eff}}$ on a large domain of volume fraction and fit $\eta_{\text{eff}}(\phi)$ with the empirical law of Krieger and Dougherty [29]. In this paper we would like to understand the effect of HIs between pairs of confined disks on $\beta$; we thus restrain ourselves to semidilute regimes where the virial expansion of $\eta_{\text{eff}}$ [Eq. (1)] is valid to order $\phi^2$.

For an infinite 3D fluid, the values of $[\eta]_\infty$ and $\beta_\infty$ are very well known. Since Einstein's seminal calculations that determined $[\eta]_\infty = 2.5$ [30,31], the contribution of HIs to $\eta_{\text{eff}}$ for non-Brownian suspensions of uniformly distributed hard spheres has been calculated by Batchelor and Green [32], who found $\beta_\infty = 5.2 \pm 0.3$. Then further accurate calculations gave a value of $\beta_\infty$ very close to 5.0 [33,34]. In two dimensions, if the Einstein viscosity $[\eta]_\infty = 2$ is a well-known value [35,36], the 2D $\beta_\infty$ value is less reported in the literature where $\beta_\infty = 4.0$ was calculated for the shear modulus of a 2D incompressible solid suspension of uniformly distributed disks [37]. This value was obtained by taking the far-field approximation for the disk-disk interactions. Here we show that the value is in fact closer to $\beta_\infty = 3.6$ with a very accurate analytical calculation.

In order to properly investigate the rheology, the suspension is submitted to a shear flow between two moving walls where no-slip boundary conditions are used. The effective viscosity is calculated by integrating the dissipation in the liquid phase. Details of the numerical 2D method based on finite elements are given below. In view of validating our simulations, we compare $[\eta]$ and $\beta$ obtained for vanishing confinements to analytical results $[\eta]_\infty$ and $\beta_\infty$. In the dilute case, i.e., for $[\eta]$, we perform very accurate analytical calculations, which give the value of $[\eta]$ in the presence of a single wall. In the semidilute case, i.e., regarding $\beta$, we numerically analyze the disk-disk HI within a uniform distribution of non-Brownian particles with a very weak confinement; we find $\beta = 3.6 \pm 0.1$, which is very close to the analytically value $\beta_\infty = 3.6$.

We find that the main source of dissipation arises in the fluid region between disks and walls. However, another important source of dissipation lies in the region between two disks that are at $45^\circ$ (mod $90^\circ$) from each other (the $0^\circ$ angle is taken from horizontal position when disks are aligned along the flow parallel to the walls). While increasing confinement, the local dissipation density increases between each disk and walls but decreases between disks because of the disappearance of $45^\circ$ configurations due to the geometrical constraint. The increase of dissipation between disks and walls is a contribution of each individual disk (i.e., it is a linear $\phi$ variation) and it increases $[\eta]$. If the latter effect can be expected, we also observe a much less predictable phenomenon: the creation

of dips of dissipation between aligned and close disks, where locally, dissipation is less than the dissipation created by the shear flow without disks. Thus, an aligned pair of disks along the flow dissipates less than two noninteracting disks: This is the contribution of pairs of disks to dissipation (i.e., a $\phi^2$ variation) and it leads to a negative contribution to the HI and explains the negativeness of $\beta$. This phenomenon finds its origin in the slowdown of the angular velocity of each disk due to their mutual interaction within the pair aligned along the flow. In light of this 2D interpretation, we check that this result holds in three dimensions.

The results of our work can be summarized as follows. (i) We use a numerical method based on a penalty function and finite elements to simulate suspensions of rigid particles. (ii) We plot the energy dissipation density for different configurations of confined disks and show how confinement and different orientations of disks affect the total dissipation. (iii) We present results for confined and unconfined 2D suspensions. (iv) We derive the Batchelor coefficient $\beta$ for unconfined 2D suspensions.

The paper is organized as follows. In Sec. II we explain the details of our numerical method. In Sec. III we show the results concerning disk-wall and disk-disk HIs. Then we compare our results with the 3D case. In Sec. IV we present analytical calculations concerning a single disk, a pair of disks, and a suspension of disks in a shear flow. We summarize in Sec. V. Details of analytical calculations of a single disk close to a wall are given in the Appendix.

## II. NUMERICAL MODEL

From the modeling point of view, our problem can be seen as a fluid-structure interaction. Therefore, it could be modeled by a coupling between Stokes equations for the dynamics of the surrounding incompressible fluid and Newton-Euler equations for the motion of rigid bodies. The action of the fluid on the particles (disks in two dimensions or spheres in three dimensions) is modeled by the hydrodynamic forces and torques acting on particles' surface, which can be considered as the right-hand side of Newton-Euler equations. In addition, particles interact with the surrounding fluid using a no-slip boundary condition in Stokes equations. However, this explicit coupling can be unstable numerically and its resolution often requires a very small time step. In addition, as we have chosen to use the finite-element method (FEM) (for accuracy reasons) and since the positions of particles change with time, we have to remesh the computational domain at each time step or in the best case at every few time steps.

For all these reasons we chose another strategy to model our problem. Instead of using Newton-Euler equations for modeling the particles' motion and Stokes equations for the fluid flow, we use only the Stokes equations in the whole domain (including the interior of the particles). We take into account the presence of particles by using a second fluid with a high viscosity on which we impose a rigid body constraint. This type of strategy is widely used in the literature under the generic names of penaltylike methods or fluid particle dynamics [38–43].

In what follows we describe briefly the basic ingredients of the FEM as well as the penalty technique applied to our problem. To do this we need to recall some mathematical notation.

The fluid flow is governed by the Stokes equations of an incompressible fluid that can be written as follows:

$$-\eta_0 \mathbf{\Delta u} + \mathbf{\nabla} p = 0 \text{ in } V_f, \tag{2}$$

$$\mathbf{\nabla} \cdot \mathbf{u} = 0 \text{ in } V_f, \tag{3}$$

$$\mathbf{u} = \mathbf{u}^\infty \text{ on } \partial V_f, \tag{4}$$

where $\eta_0$, $\mathbf{u}$, and $p$ are the viscosity, the velocity field, and the pressure, respectively, and $V_f$ is the domain occupied by the fluid. Typically $V_f = V \setminus B$ if we denote by $V$ the whole domain and by $B$ the rigid particles' domain, $\partial V_f$ is the border of $V_f$, and $\mathbf{u}^\infty$ is some given vector field for the boundary conditions (typically a velocity field representing the shear flow). It is known that under some reasonable assumptions the problem (2)–(4) has a unique solution $(\mathbf{u}, p)$ [44].

As we will use the FEM for the numerical resolution of the problem (2)–(4), we need to write its variational formulation. For the sake of simplicity, we start by writing it in a standard way (fluid without particles) and then we modify it using the penalty technique to take into account the presence of particles. In what follows we describe briefly these two methods, the standard variational formulation for the Stokes problem, and the penalty technique to handle the rigid body motion of particles.

### A. Variational formulations

The variational formulation of our initial problem (2)–(4) is given as follows: Find $(\mathbf{u}, p)$ (see the Appendix of [45] for more details) such that

$$2\eta_0 \int_{V_f} \boldsymbol{\tau}(\mathbf{u}) : \boldsymbol{\tau}(\mathbf{v})\, dV - \int_{V_f} p \nabla \cdot \mathbf{v}\, dV = 0 \,\forall \mathbf{v}, \tag{5}$$

$$\int_{V_f} q \nabla \cdot \mathbf{u}\, dV = 0 \,\forall q, \tag{6}$$

$$\mathbf{u} = \mathbf{u}^{\infty} \text{ on } \partial V_f, \tag{7}$$

where $\boldsymbol{\tau}(\mathbf{u})$ is the strain tensor

$$\boldsymbol{\tau}(\mathbf{u}) = \tfrac{1}{2}[\nabla \mathbf{u} + (\nabla \mathbf{u})^t] \tag{8}$$

and $\mathbf{v}$ and $q$ are, respectively, the test functions for the velocity field $\mathbf{u}$ and the pressure $p$ taken in some functional space (see [45]). As we have Dirichlet boundary conditions (7), $\mathbf{v}$ is supposed to vanish on $\partial V_f$.

The variational formulation (5)–(7) has the advantage of depending explicitly on $\boldsymbol{\tau}(\mathbf{u})$, which will be very useful in handling the rigid body motion. Note that this formulation is equivalent to the classical one due to the identity

$$\int_{V_f} \boldsymbol{\tau}(\mathbf{u}) : \boldsymbol{\tau}(\mathbf{v})\, dV = \frac{1}{2} \int_{V_f} \nabla \mathbf{u} : \nabla \mathbf{v}\, dV, \tag{9}$$

which holds for incompressible fluid. All details of calculations to obtain these variational formulations can be found in Ref. [45].

### B. Penalty method

We now briefly describe the penalty strategy in the framework of the FEM (see [38,39] for more details). The first step consists in rewriting the variational formulation (5)–(7) by replacing the integrals over the real domain occupied by the fluid ($V_f = V \setminus B$) by those over the whole domain $V$ (including the particles $B$). This simply means that we extend the solution $(\mathbf{u}, p)$ to the whole domain $V$. More precisely, the penalty method replaces the particles by an artificial fluid with a high viscosity. This is made possible by imposing a rigid body motion constraint on the fluid that replaces the particles [$\boldsymbol{\tau}(\mathbf{u}) = 0$ in $B$]. Obviously, the divergence-free constraint is also ensured in $B$. The problem (5)–(7) is then modified as follows: Find $(\mathbf{u}, p)$ such that

$$2\eta_0 \int_V \boldsymbol{\tau}(\mathbf{u}) : \boldsymbol{\tau}(\mathbf{v}) dV + \frac{2}{\varepsilon} \int_B \boldsymbol{\tau}(\mathbf{u}) : \boldsymbol{\tau}(\mathbf{v}) dV - \int_V p \nabla \cdot \mathbf{v}\, dV = 0 \,\forall \mathbf{v}, \tag{10}$$

$$\int_V q \nabla \cdot \mathbf{u}\, dV = 0 \,\forall q, \tag{11}$$

$$\mathbf{u} = \mathbf{u}^{\infty} \text{ on } \partial V, \tag{12}$$

where $\varepsilon = 10^{-6}$ is the penalty parameter.

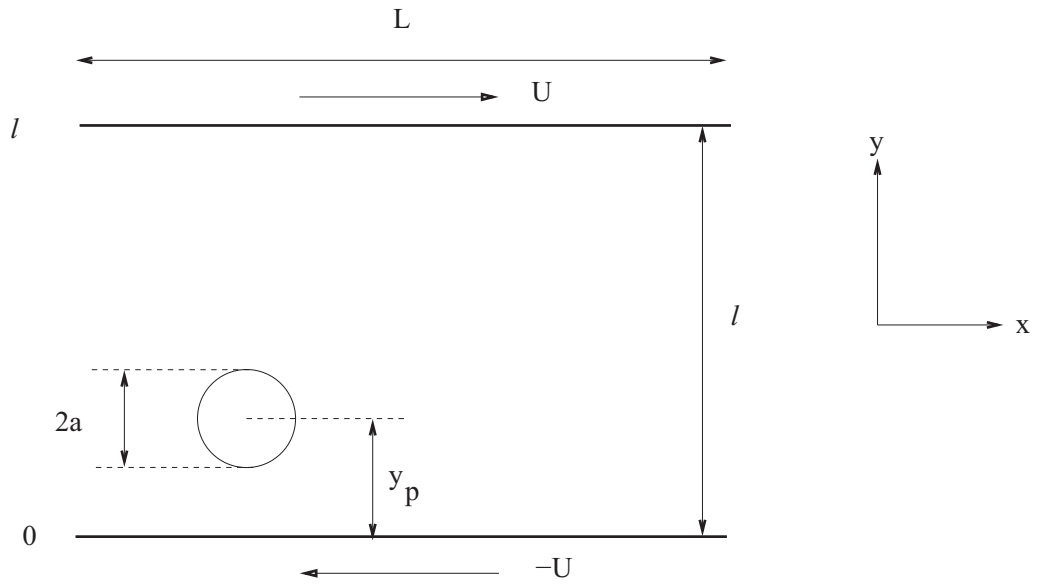


FIG. 1. Circular particle in a linear shear flow in the presence of walls. The shear rate is $\dot{\gamma} = 2U/\ell$ and it is maintained at $\dot{\gamma} = 1$ in the simulations.

Finally, if we denote the time discretization parameter by $t_n = n\delta t$, the velocity and the pressure at time $t_n$ by $(\mathbf{u}_n, p_n)$, the velocity of a particle at time $t_n$ by $\mathbf{W}_n$, and the position of its center by $\mathbf{X}_n$, we can write our algorithm as

$$\mathbf{W}_n = \frac{1}{\mathcal{V}(B)} \int_B \mathbf{u}_n dV, \tag{13}$$

$$\mathbf{X}_{n+1} = \mathbf{X}_n + \delta t \mathbf{W}_n, \tag{14}$$

where $\mathcal{V}$ denotes volume. Further, $(\mathbf{u}_{n+1}, p_{n+1})$ solves

$$2\eta_0 \int_V \boldsymbol{\tau}(\mathbf{u}_{n+1}) : \boldsymbol{\tau}(\mathbf{v}) dV + \frac{2}{\varepsilon} \int_B \boldsymbol{\tau}(\mathbf{u}_{n+1}) : \boldsymbol{\tau}(\mathbf{v}) dV - \int_V p_{n+1} \nabla \cdot \mathbf{v}\, dV = 0, \tag{15}$$

$$\int_V q \nabla \cdot \mathbf{u}_{n+1} dV = 0, \tag{16}$$

$$\mathbf{u}_{n+1} = \mathbf{u}^\infty \text{ on } \partial V. \tag{17}$$

This algorithm is valid for any dimension. Here it has been implemented in two dimensions using a user-friendly FEM software FREEFEM++ [46].

In our problem, the $x$ axis is parallel to the flow direction and the $y$ axis is perpendicular to the walls (see Fig. 1). We apply periodic boundary conditions along $x$. We checked that starting with a uniform distribution and incrementing particle positions as mentioned above [Eq. (14)] does not change the pair distribution function (data not shown) along time. The suspension remains uniform on a time scale equal to the time necessary for a particle close to a wall to cross the simulation box several times. Keeping a uniform distribution is essential to compare numerical and analytical results for the $\beta$ coefficient. The concentrations studied are rather low (we are interested in semidilute regimes) where interactions between pairs of particles and between each particle and walls becomes non-negligible and contribute to the global dissipation. Thus, we do not add any short-range repulsive forces. At these concentrations (below 15%) Stokes repulsion is indeed enough to avoid any spurious overlapping.

## III. NUMERICAL RESULTS

### A. Particle-wall interaction: Dilute case

In this section we consider a single rigid circular particle in a confined shear flow (see Fig. 1). The shear rate $\dot{\gamma}$ is maintained equal to 1 for all the simulations. The whole mesh is composed of 8000 triangles and each disk is represented by approximately 70 elements. The velocity field $\mathbf{u}$ is approximated by finite elements of degree 2 ($\mathbb{P}_2$) and the pressure is approximated by linear finite elements ($\mathbb{P}_1$). Finally, we use free boundary conditions in the $x$ direction.

The box is large enough ($L/\ell = 60$) so that no boundary effects are present in the $x$ direction and the wall interdistance $\ell$ is varied in order to study the effect of the confinement. The volume fraction is then $\phi = \pi a^2/L\ell$. Since the $x$ dimension of the system is very long compared to the $y$ one, the effective viscosity of this system should depend only on the dimensionless distance from the wall $\tilde{y} = y_p/\ell$ and on the confinement $C = a/\ell$. The total dissipation is

$$D = \frac{1}{2}\eta_0 \int_V |\nabla \mathbf{u} + \nabla \mathbf{u}^t|^2 dV, \tag{18}$$

where $\mathbf{u}$ is the velocity field in the fluid phase as well as in the disk. Inside disks, due to their solid motion, there is no dissipation and the integral holds on the whole domain (fluid and particles). In the spirit of homogenization, we consider a homogeneous Newtonian fluid of viscosity $\eta_{\text{eff}}$. The total dissipation is then

$$D = \eta_{\text{eff}} \dot{\gamma}^2 L\ell. \tag{19}$$

This equation defines the equivalence between total dissipation and effective viscosity at a given $\dot{\gamma}$, $L$, and $\ell$. From Eqs. (18) and (19) we get

$$\eta_{\text{eff}} = \frac{\eta_0}{2\dot{\gamma}^2 L\ell} \int_V |\nabla \mathbf{u} + \nabla \mathbf{u}^t|^2 dV. \tag{20}$$

Using the stresslet of each particle, the 2D effective viscosity can be expressed in term of the average extra particle stress $\sigma_{xy}^S$ [36] of the suspension:

$$\eta_{\text{eff}} = \eta_0 \left(1 + \frac{\phi}{\pi a^2 \eta_0 \dot{\gamma}} \sigma_{xy}^S\right), \tag{21}$$

where $\sigma_{xy}^0 = \eta_0 \dot{\gamma}$.

For a dilute ($\phi \to 0$) and not confined 2D suspension, the stresslet is such that

$$\sigma_{xy}^S = 2\pi a^2 \eta_0 \dot{\gamma}, \tag{22}$$

leading to the well-known 2D result $\eta_{\text{eff}} = \eta_0(1 + 2\phi)$ [35,36]. The so-called Einstein viscosity is given by

$$[\eta](\tilde{y}, C) = \lim_{\phi \to 0} \frac{\eta_{\text{eff}} - \eta_0}{\eta_0 \phi} \tag{23}$$

and is directly related to the extra particle stress by $[\eta] = \lim_{\phi \to 0} \sigma_{xy}^S / \pi a^2 \eta_0 \dot{\gamma}$ for any confinement. Therefore, calculating the Einstein viscosity or the stresslet for vanishing $\phi$ values is the same task. Note that for a semidilute suspension, hydrodynamic interactions make the stresslet depend on $\phi$. Regarding the disk position, the problem is symmetrical with respect to the center of the channel ($\tilde{y} = 1/2$). Thus, we can restrict our study to the range $\ell/2 < y_p < \ell - a$ (i.e., $1/2 < \tilde{y} < 1 - C$). The simulations consist of setting a disk at different $\tilde{y}$ in the channel in the range given above and calculating the effective viscosity.

Figure 2 shows the results for several distances from the wall and for several confinements. When the disk approaches the wall, the viscosity of the system increases. The curve becomes steeper when

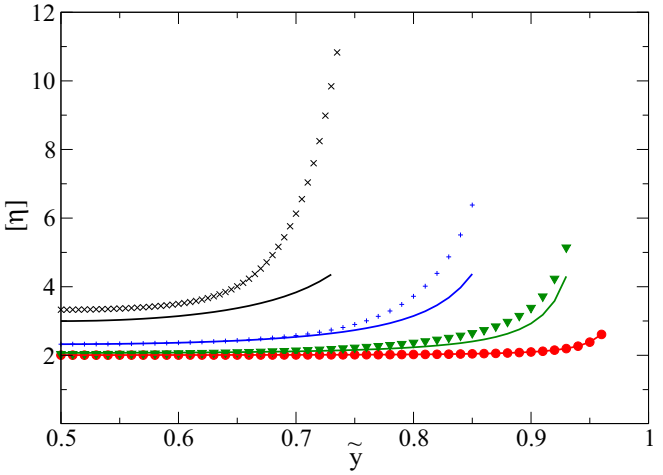


FIG. 2. Einstein viscosity depending on the dimensionless vertical position $\tilde{y}$ for several confinements. For small confinements, when the disk is close to the middle of the channel ($\tilde{y} \approx 0.5$) the asymptotic value $[\eta] = 2$ is recovered. For stronger confinements, even when the disk is centered ($\tilde{y} \approx 0.5$), we get $[\eta] > 2$. The confinement $C = 0.022$ (red circles), $C = 0.0665$ (green triangles), $C = 0.143$ (blue pluses), and $C = 0.25$ (black crosses). The analytical expansion [Eq. (25)] is represented by solid curves.

the disk is closer to the wall. For small confinement values, we recover $[\eta] = 2$, consistent with exact 2D values [35,36]. For intermediate confinements, the stresslet is higher near the wall; $[\eta]$ decreases to 2 when approaching the center of the channel. It is interesting to note that for strong confinements, the viscosity never decreases to the limit $[\eta] = 2$ for a centered disk. This means that for strong confinements, the presence of walls cannot be neglected for any position of the disk.

For asymptotic cases (i.e., small confinements), it is possible to compare our numerical results with an analytical expression of $[\eta]$. We analytically calculate $[\eta]$ for a given distance between the disk and the walls. We made an expansion similar to the one done in Ref. [47] where we consider the problem of a single circular particle near a single wall. The fluid is considered as infinite along the $x$ direction and semi-infinite along $y$. One can expand the velocity field $\mathbf{u}(x, y)$ as a polynomial function of the dimensionless distance between the center of the disk and the wall: $h_0 = (\ell - y_p)/a = (1 - \tilde{y})/C$. The reflection method [47] is employed to satisfy boundary conditions at the wall. We find the solution for $\mathbf{u}$ by using Eq. (23). We stop the expansion at sixth order and it reads [the expansion valid to order $o(1/h_0^{12})$ is given in the Appendix]

$$[\eta]_{1\,\mathrm{wall}}(h_0) = 2 + \frac{2}{h_0^2} - \frac{1}{4h_0^4} + \frac{15}{16h_0^6} + o\big(1/h_0^6\big). \tag{24}$$

Adding the reflection from the second wall, we get

$$[\eta]_{2\,\mathrm{walls}} = [\eta]_{1\,\mathrm{wall}}(h_0) + [\eta]_{1\,\mathrm{wall}}(h_1) - 2, \tag{25}$$

where $h_1 = \tilde{y}/C$. In Fig. 2, Eq. (25) fits very well the numerical data for small confinements: The model is valid for $\tilde{y} < 0.7$ and $C < 0.143$. Note that higher reflections with two walls should be added in order to refine the expressions (24) and (25). Here our objective is to compare our numerical results with simple asymptotic expansions.

For dilute suspensions, the contribution of each disk to $[\eta]$ is simply added. Thus, for a suspension of $N$ identical disks whose positions are known, one can express the Einstein viscosity of the whole

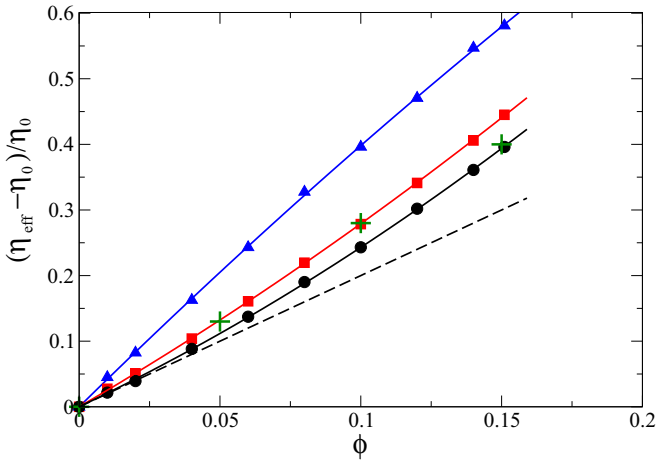


FIG. 3. Relative effective viscosity as a function of the volume fraction $\phi$ for several values of confinement: $C = 0.01$ (black circles), $C = 0.13$ (red squares), and $C = 0.286$ (blue triangles). Solid curves are the fits done with Eq. (1). For $C = 0.01$, $[\eta] = 2.0$, and $\beta = 3.6$; for $C = 0.12$, $[\eta] = 2.4$, and $\beta = 3.2$; and for $C = 0.3$, $[\eta] = 4.2$, and $\beta = -2.0$. We clearly see an increase of Einstein viscosity $[\eta]$ (slope at the origin) and a decrease and even a negative value of the curvature $\beta$ when increasing confinement. The results of Dodd *et al.* [6] (green pluses) obtained for $C \to 0$ are represented for comparison. The Brady result [36] linear in $\phi$ is represented by the dashed curve.

suspension as

$$[\eta](C) = \frac{1}{N}\sum_{i=1}^{N}[\eta](\tilde{y}_i, C), \tag{26}$$

where $\tilde{y}_i = y_{p,i}/\ell$ is the dimensionless vertical position of the $i$th disk.

This first part of our work allows us to see that the main contribution of each individual disk to the effective viscosity is due to the increase of dissipation between each disk and walls. We now examine denser suspensions, to understand the role of hydrodynamic interactions inside pairs of disks.

### B. Disk-disk hydrodynamic interactions between two walls

Upon increasing the volume fraction $\phi$, hydrodynamic interactions between pairs of disks start to contribute to the total dissipation [$\beta$ term of Eq. (1)]. In three dimensions it was shown [19–21] that $\beta$ decreases for intermediate confinements and even becomes negative for stronger confinements. As shown in this paper, the same effect arises in two dimensions.

We calculate the relative effective viscosity as a function of volume fraction for several values of confinement ranging from $C = 0.01$ to $C = 0.45$ (see Fig. 3 for some specific chosen confinement values). We clearly see a negative curvature of the curves $\eta_{\text{eff}}(\phi)$ for strong confinements. We fit these curves with a second-order polynomial as in Eq. (1) and obtain values of $[\eta]$ and $\beta$ as a function of $C$. Note that we do this fit for values of $\phi$ below $\phi_{\max} = 12\% \pm 2\%$ where no third-order contribution in $\phi$ is necessary to fit the data. We vary a bit $\phi_{\max}$ from 10% to 14% as well as disk configurations in order to evaluate the uncertainty on $[\eta]$ and $\beta$. In Fig. 4 we see the increase of $[\eta]$ as a function of $C$ and the decrease of $\beta$ as well as its sign change for strong confinements. Note that for stronger confinements, $\beta$ increases again to 0 asymptotically. For small confinement values (i.e., $C = a/\ell \to 0$) we asymptotically reach the following values for an infinite fluid: $[\eta]_\infty = 2$ and $\beta_\infty = 3.6 \pm 0.1$. These numerical values are in perfect agreement with the reported value of the

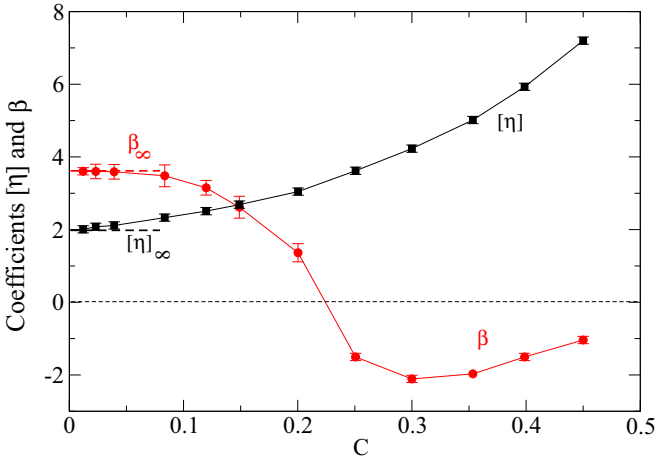


FIG. 4. Coefficients $[\eta]$ (black squares) and $\beta$ (red circles) as a function of confinement $C$. The error bars are calculated from several fits done with different maxima of the volume fraction (see the text). Values of $[\eta]_\infty$ and $\beta_\infty$ are indicated by horizontal dashed lines.

literature, $[\eta]_\infty = 2$ in two dimensions [35,36], and with our own analytical result, $\beta_\infty = 3.6$ (see Sec. IV).

Since it is much more convenient to represent the velocity field in two dimensions as well as the dissipation density, we can easily give an interpretation of our results. Figure 5 shows the dissipation density field $\delta = \frac{1}{2}\eta_0|\nabla\mathbf{u} + \nabla\mathbf{u}^t|^2$ for a suspension of disks that are randomly distributed between the walls. Dissipation density around a single disk has an angular distribution with maxima at $\pi/4$ (mod $\pi/2$) with flow direction (the $x$ axis) (Fig. 5) (see Sec. IV). Therefore, it is not surprising that each pair of disks dissipates energy with the same kind of symmetry, i.e., along the axis of extension

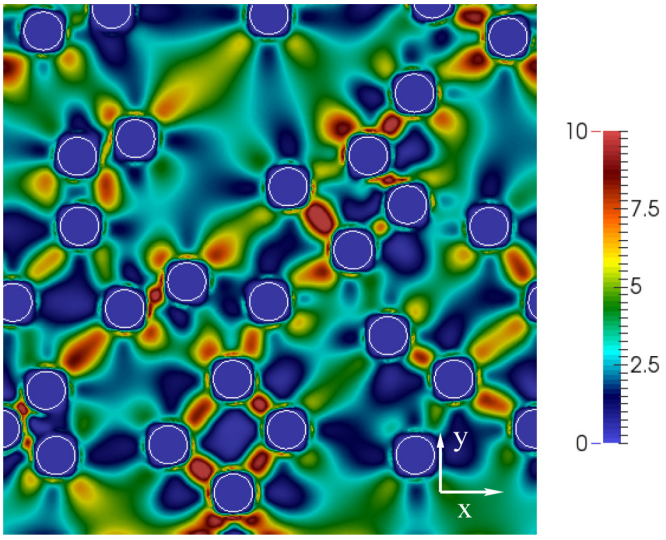


FIG. 5. Dissipation density for a given disk configuration for $C = 0.012$ (partial view of the simulation box). Dissipation is strong between close disks at 45° with $x$ axis. The color scale indicates dissipation values on an arbitrary scale from 1 to 10. The density of dissipation without disks is 3.

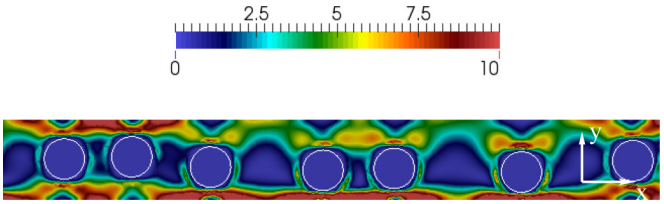


FIG. 6. Dissipation density for a given disk configuration for $C = 0.25$ (partial view of the simulation box along $x$). Dissipation is stronger between disks and walls and there are fewer disks at 45° due to the confinement. Note the dips of dissipation between disks. The color scale indicates dissipation values on an arbitrary scale from 1 to 10. The density of dissipation without disks is 3.

and compression of the shear flow, i.e., at $45^\circ \pmod{90^\circ}$ with flow direction (see Fig. 5). Along $x$ and $y$, pairs dissipate much less.

Then, by increasing the confinement, we observe an increase of dissipation between each particle and walls (see Fig. 6) and a decrease of dissipation between particles since the number of configurations with two close particles at $45^\circ \pmod{90^\circ}$ obviously decreases while the number of configurations of aligned particles along $x$ axis increases for higher confinements. Thus, by increasing $C$, particle-wall dissipation tends to increase the Einstein viscosity $[\eta]$ since it is due to each individual particle while dissipation inside pairs tends to decrease the contribution of HIs to the effective viscosity and makes $\beta$ decrease. Now we study the dissipation density around a pair of particles as well as the total dissipation.

In order to evaluate the dissipation $D$ as a function of the pair orientation in the shear flow, we consider two confined disks and vary the angle $\theta$ between the line joining each disk center and the $x$ axis (see Fig. 7). We calculate the dissipation $D$ on the whole simulation box by using Eq. (18). Since $\eta_{\text{eff}}(\phi) = D/\dot{\gamma}^2 L\ell$, by using Eqs. (1) and (26) to calculate $[\eta]$, we can calculate $\beta$ as a function of the angle $\theta$. This confirms (Fig. 8) that the maximum of dissipation (i.e., maximum of effective viscosity) occurs at 45° (when this configuration is possible according to the confinement value). Figure 8 also highlights that when red centers of disks are close to an alignment along the $x$ axis, i.e., for $\theta < 20^\circ$ and $\theta > 160^\circ$, negative values of $\beta$ are obtained. Note that for $80^\circ < \theta < 100^\circ$, we also obtain a negative value for $\beta$, but much smaller than for aligned disks. It is clear that for disks aligned along $x$ or $y$, the dissipation between the disks is smaller than the dissipation without disks. The presence of walls forces the disks to be aligned along $x$.

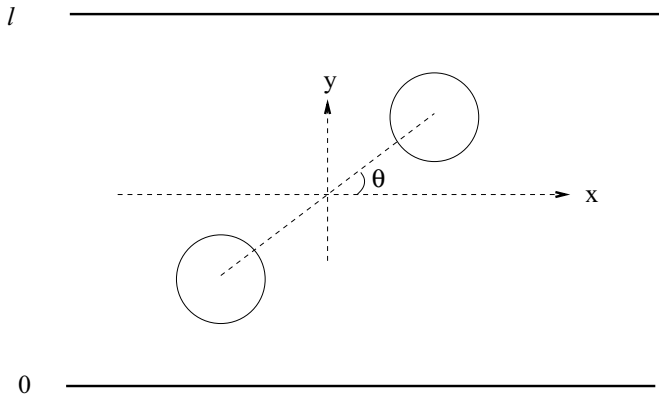


FIG. 7. Pair of disks. The line joining their centers makes an angle $\theta$ with the $x$ axis. Dissipation is integrated inside the whole simulation box and $\theta$ is varied.

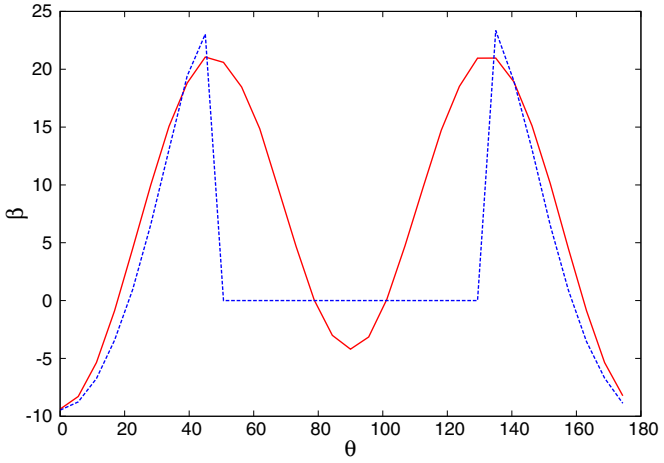


FIG. 8. Parameter $\beta$ in the case of two disks as a function of $\theta$ for $C = 0.25$ (red solid curve) and $C = 0.29$ (blue dashed curve). Concerning $C = 0.29$, the discontinuity means that orientations 50°–130° are not possible due to the confinement. Note the negative values of $\beta$ (see the text).

These results are supported by the visualization of the dissipation density and stream lines around the disks. For a pair of disks making an angle of 45° with the $x$ axis, we observe an increase of dissipation density between the disks [Fig. 9(a)]. It is due to two vortices that rotate in the same direction [Fig. 9(b)]. It creates a zone of strong shear at their intersection, which dissipates a great deal. For a pair of disks with their centers aligned along the flow (i.e., along the $x$ axis), we observe the formation of a compression and extension flow between the two disks [see Fig. 10(b)] in the dip of dissipation density.

The dissipation density between two disks aligned along the flow is smaller than the background density dissipation (i.e., the dissipation of the flow without disks $\delta_0 = \eta_0 \dot{\gamma}^2$). The origin of this local decrease of dissipation density is due to the slowdown of angular velocity $\Omega$ of the disks when aligned along the flow due to their mutual HI (see Fig. 11): Rotation of each disk slows down rotation of its neighbor. This slowdown leads to a screening of the imposed shear rate and of the associated dissipation density between two aligned disks. Note that in Fig. 11 disks are weakly confined ($C = 0.04$). It has been shown before [21] that the confinement also decreases the angular velocity of each disk. This tends to increase the screening effect of the imposed shear rate between

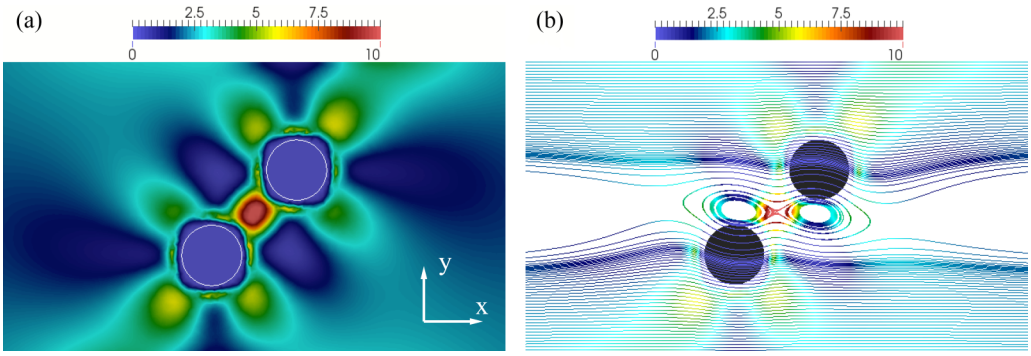


FIG. 9. (a) Dissipation density and (b) current lines and dissipation between two weakly confined disks (colored in black) positioned at 45° with the $x$ axis. Confinement is $C = 0.044$ (partial view of the simulation box). The color scale indicates dissipation values on both figures. The density of dissipation without disks is 3.

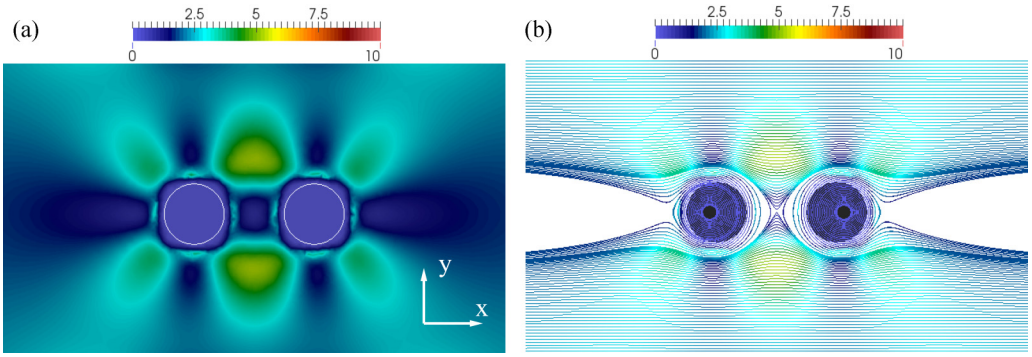


FIG. 10. (a) Dissipation and (b) current lines and dissipation between two weakly confined and aligned disks along the $x$ axis (colored in black) with $C = 0.044$ (partial view of the simulation box). The color scale indicates dissipation values in both figures. The density of dissipation without disks is 3. Dissipation is clearly weaker than in the case of disks positioned at 45° with the $x$ axis (Fig. 9).

aligned disks. On the contrary, when disks are close enough but $y$ shifted (meaning that the disks do not have the same $y$ coordinates), their angular velocity is bigger than when they are far apart (see Fig. 11).

The fluid region between two close disks aligned along the flow has a smaller dissipation than the one imposed by the motion of walls without disks. It represents a dip of dissipation, which contributes to decrease the total dissipation for aligned pairs of disks compared to two isolated single disks. Indeed, in Fig. 12 we can observe the evolution of the dissipation density profile between two disks in a shear flow (the pair being aligned along the flow). A dip of dissipation is created between the disks and increases when the disks get closer. This explains why the pair interaction (when the pair of disks is aligned along the flow) contributes negatively to the effective viscosity. Note that the

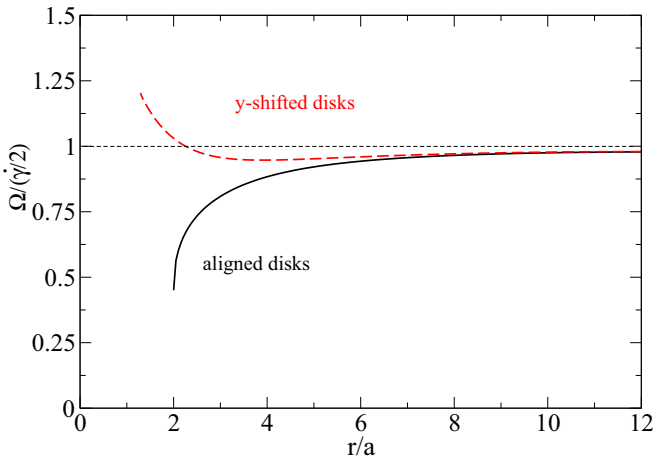


FIG. 11. Pair of disks within a shear flow. The angular velocity Ω of each disk divided by $\dot{\gamma}/2$ is plotted as a function of the disk interdistance $r/a = (x^2 + y^2)^{1/2}/a$. While $y$ is fixed, $x$ is varied. The red dashed curve shows shifted disks along $y$ (meaning that the disks do not have the same $y$ coordinates). Particles are symmetrically shifted from the center of the flow and their $y$ interdistance is $2.5a$. The black solid curve shows aligned disks along $x$ ($y = 0, \theta = 0°$). Note that for large interdistances, in both cases Ω does not tend to $\dot{\gamma}/2$ but to a slightly smaller value. This is due to the confinement effect (here $C = 0.044$).

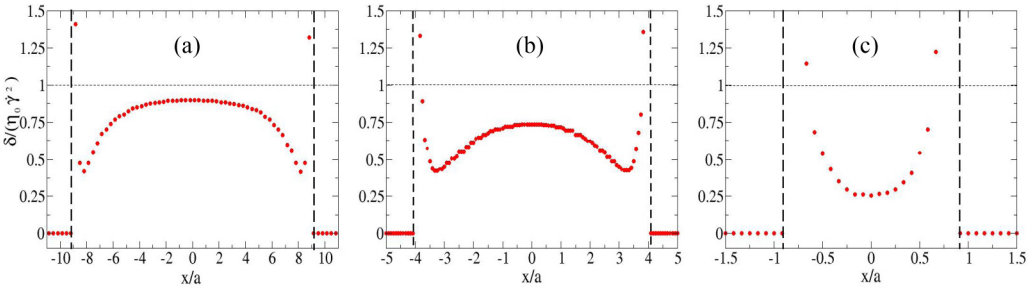


FIG. 12. Dimensionless dissipation density $\delta/\eta_0\dot{\gamma}^2$ between two disks along $x$. The centers of the disks are aligned along the $x$ axis with the same $y$ coordinate. The confinement is $C = 0.04$. The vertical dashed lines indicate the disk-fluid interfaces $\delta = 0$ inside the disks (rigid particles). The interdistance $2x_0/a$ between the centers of the disks is varied: (a) $x_0/a = \pm 10.15$, (b) $x_0/a = \pm 5.1$, and (c) $x_0/a = \pm 1.8$. We clearly see that the dip of dimensionless dissipation density between the disks is enhanced when disks are closer. Note that $\delta/\eta_0\dot{\gamma}^2$ is below one.

confinement is weak in Fig. 12; somehow the confinement forces the aligned configuration where dips of dissipation occur and makes $\beta$ decrease to negative values.

The increasing again of $\beta$ as a function of $C$ (Fig. 4) is explained by the fact that when confinement is increased, the relative distance between disks increases in order to stay in the limit $\phi < 12\%$. Therefore, the contribution of HIs between disks decreases ($\beta \to 0$).

### C. Comparison with the 3D case

In order to confirm our observations in two dimensions, we made simulations in three dimensions, which are much less convenient to perform because of the time and memory consumption as well as the flow field representation. In Fig. 13 we schematically represent two confined spheres located in a plane parallel to the walls.

This is the situation that is relevant for confined configurations. The line joining the centers of the spheres makes an angle $\varphi$ with the shear plane ($xOz$ plane). In Fig. 14(a) we set two aligned spherical particles in the shear plane ($\varphi = 0^\circ$) and calculate their dissipation density in the plane

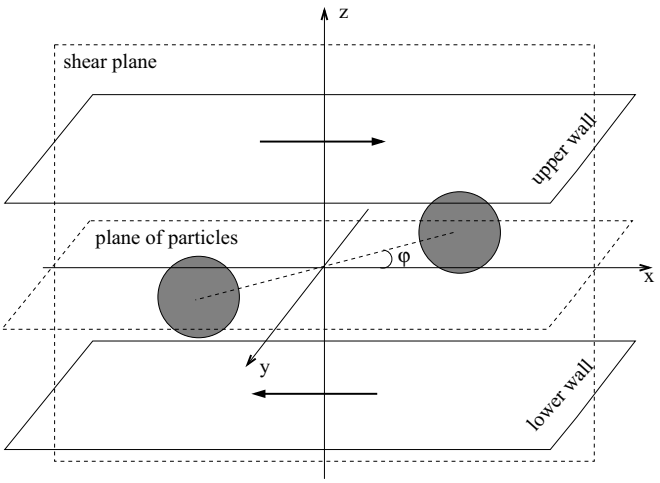


FIG. 13. Two spheres confined in a shear flow. The centers of the spheres are in the same plane parallel to the walls.

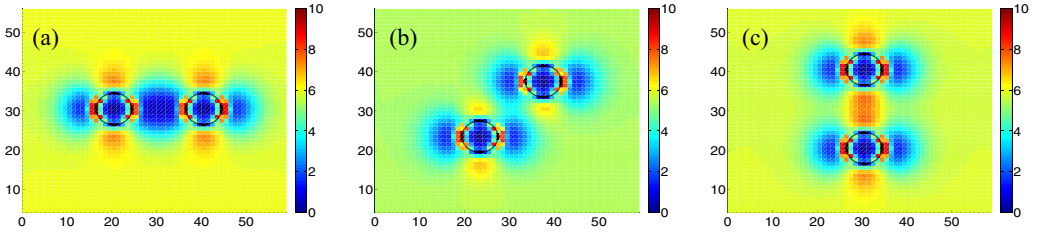


FIG. 14. Dissipation density in the $xOy$ plane between two spherical particles as a function of $\varphi$ for a confinement $C = 0.25$ and (a) $\varphi = 0^\circ$, (b) $\varphi = 45^\circ$, and (c) $\varphi = 90^\circ$. The nonuniform dissipation field inside spheres is due to discretization effect.

containing the sphere centers ($xOy$). Here also, a dip of dissipation is obtained between the two spheres [see Fig. 14(a)]. When the line joining the centers of the confined spheres makes an angle $\varphi = 45^\circ$ with the shear plane [see Fig. 14(b)], no increase of dissipation density is observed between the spheres. In addition, when $\varphi = 90^\circ$, a maximum of dissipation density is observed between the two spheres [see Fig. 14(c)]. However, a careful averaging on the different configurations (i.e., from $\varphi = 0^\circ$ to $\varphi = 180^\circ$) shows that the contribution of aligned spheres dominates and leads to a decrease of dissipation for confined pairs of spheres. So, even if 3D simulations require additional unavoidable averaging on different configurations, we see that, qualitatively, the same interpretation can be found in three and two dimensions.

## IV. ANALYTICAL APPROACH

### A. Single disk in a shear flow

The problem of a single disk in shear flow can be fully solved analytically. In this section we use the coordinate system $(x,y)$ such that the shear flow is written as $\boldsymbol{v}^\infty(x,y) = \dot\gamma \boldsymbol{e_x} y$. For convenience, we represent 2D vectors as complex numbers in order to simplify the notation. For example, the position will be written as $\zeta = x + iy$ and the velocity $\boldsymbol{u}(x,y)$ will be written as $\xi(\zeta) = u_x(x,y) + iu_y(x,y)$. It is generally known [48] that a solution of the Stokes equations (2) and (3) can be written as

$$\xi(\zeta) = A(\zeta) - \zeta\overline{A'(\zeta)} + B(\overline{\zeta}), \tag{27}$$

where the $A(\zeta)$ and $B(\zeta)$ functions that are analytical inside the fluid and the upper bar stand for the complex conjugate. The undisturbed shear flow is written as

$$u_x^\infty(x,y) + iu_y^\infty(x,y) = \frac{\dot\gamma(z-\overline{z})}{2i}. \tag{28}$$

Placing a rigid disk of radius $a$ in the origin results in the following expression of the flow outside the disk:

$$\xi(\zeta) = \frac{\dot\gamma(z-\overline{z})}{2i} - \frac{i\dot\gamma a^2}{2z} + \frac{i\dot\gamma a^2 z}{2\overline{z}^2} - \frac{i\dot\gamma a^4}{\overline{z}^3}. \tag{29}$$

It is easy to check that expression (29) is of the form (27) and that the velocity at the disk boundary corresponds to rotation with angular velocity $-\dot\gamma/2$. The dissipation density $\delta$ corresponding to the flow (29) is

$$\delta(\zeta) = \dot\gamma^2\eta_0\left(1 + 4\frac{a^4}{|\zeta|^4} - \frac{12a^6}{|\zeta|^6} + \frac{9a^8}{|\zeta|^8} - \frac{2a\zeta}{\overline{\zeta}^3} - \frac{2a^2\overline{\zeta}}{\zeta^3} + \frac{3a^4}{\zeta^4} + \frac{3a^4}{\overline{\zeta}^4}\right). \tag{30}$$

Writing $\zeta = |\zeta|e^{i\alpha}$, we observe that the angular dependence of $\delta$ has the form of $\delta(\zeta) = \delta_0(|\zeta|) + \delta_4(|\zeta|)\cos 4\alpha$.

### B. Hydrodynamic interaction of two disks in unconfined shear flow

In order to calculate the the Batchelor coefficient for a 2D suspension of rigid disks, it is first necessary to evaluate the hydrodynamic interactions of two disks as a function of the vector $\boldsymbol{r}$ separating their centers. For convenience, we put the particles in positions $\boldsymbol{r}/2$ and $-\boldsymbol{r}/2$. The symmetry of the problem dictates that $\xi(\zeta) = -\xi(-\zeta)$. The flow disturbance $\xi_1(\zeta)$ due to a force-free disk with the center at position $\zeta_0 = (r_x + ir_y)/2$ can be written as a multipolar expansion

$$\xi_1(\zeta + \zeta_0) = \sum_{k=1}^{\infty} \frac{A_k}{\zeta^k} + \frac{k\overline{A_k}\zeta}{\overline{\zeta}^{k+1}} + \frac{B_k}{\overline{\zeta}^k}. \tag{31}$$

The expansion (31) converges everywhere for $|\zeta| > a$ ($a$ being the disk radius as defined above), including infinity, where the flow disturbance is equal to zero. Were there a force acting on the disk, the expansion (31) would contain a logarithmic singularity in the disk center. Accounting for the symmetry of the problem, the velocity disturbance due to the second disk can be expressed as $\xi_2(\zeta) = -\xi_1(-\zeta)$. The total flow field outside of the disks is the sum of the flow disturbance due to each disk and the unperturbed shear flow at infinity $\xi^\infty = i\dot{\gamma}(\overline{\zeta} - \zeta)/2$:

$$\xi(\zeta) = \xi_1(\zeta + \zeta_0) - \xi_1(-\zeta - \zeta_0) + \xi^\infty(\zeta). \tag{32}$$

The coefficients $A_k$ ($k > 0$) and $B_k$ ($k > 1$) are calculated from the no-slip boundary condition at the disks' boundaries

$$\xi(\zeta_0 + ae^{i\sigma}) = \xi_0 + i\Omega e^{i\sigma}, \tag{33}$$

where $\sigma \in \mathbb{R}$ is the parametrization of the boundary of the disk, $\xi_0$ is the velocity of the disk located at $\boldsymbol{r}/2$, and $\Omega$ is its angular velocity. The condition of (33) is reduced to a discrete (albeit infinite) linear system by projecting on the space of Fourier harmonics $e^{ik\sigma}$. This system is closed by the zero-torque condition $\Im B_1 = 0$. The resulting system is solved for the approximate values of $A_k$ and $B_k$ by assuming that each unknown has an analytical expansion in powers of the small parameter $2a/r$. Truncating all calculations to a proper degree of $2a/r$ allows us to calculate the coefficients in each expansion. We do not give here the resulting calculations. Instead, we list below several first terms in the expansion for each parameter of interest, which can serve as a basis of an independent validation of our study. The parameters of interest are the velocity $\xi_0$, the angular velocity $\Omega$, and the coefficient $A_1$. The latter is closely related to the stress generated in suspension. In particular, $-4\Im A_1/S\dot{\gamma}$ is the contribution of the particle to the effective viscosity of the suspension, as will be explained in the next section. Figure 15 shows the extra particle stress around a disk in the presence of another one:

$$\Re\xi_0^{\mathrm{pw}} = \dot{\gamma}\left[\frac{r\sin\theta}{2} - \frac{a^2(\sin 3\theta + \sin\theta)}{2r} + \frac{a^4(\sin 3\theta - 2\sin\theta)}{2r^3} + o((a/r)^3)\right], \tag{34}$$

$$\Im\xi_0^{\mathrm{pw}} = \dot{\gamma}\left[\frac{a^2(\cos 3\theta - \cos\theta)}{2r} - \frac{a^4(\cos 3\theta + 2\cos\theta)}{2r^3} + o((a/r)^3)\right], \tag{35}$$

$$\Omega^{\mathrm{pw}} = \dot{\gamma}\left[-\frac{1}{2} + \frac{a^2\cos 2\theta}{2r^2} - \frac{2a^4\cos 2\theta}{r^4} + o((a/r)^4)\right], \tag{36}$$

$$\Re A_1^{\mathrm{pw}} = \dot{\gamma}\left[-\frac{a^4\sin 4\theta}{r^2} + \frac{3a^6\sin 4\theta}{r^4} + o((a/r)^4)\right], \tag{37}$$

$$\Im A_1^{\mathrm{pw}} = \dot{\gamma}\left[-\frac{a^2}{2} - \frac{a^4\cos 4\theta}{r^2} - \frac{a^6(2 + 3\cos 4\theta)}{r^4} + o((a/r)^4)\right]. \tag{38}$$

Here all expressions refer to the disk located at $\boldsymbol{r}/2$ and the superscript pw is added to stress that the values are calculated for the pairwise interaction of two disks.

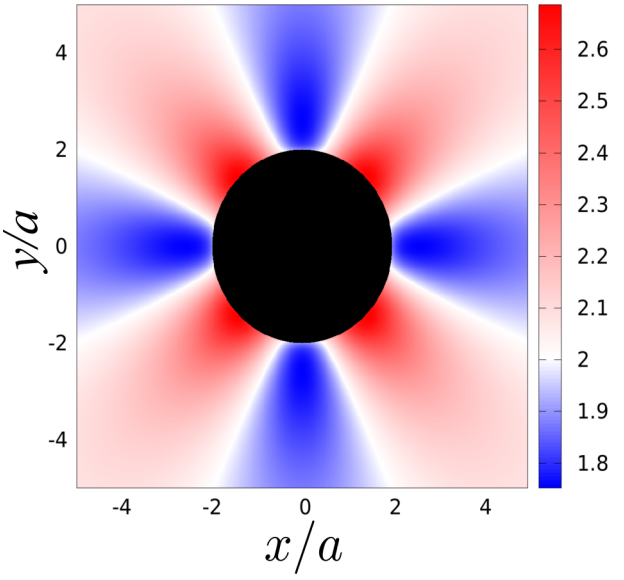


FIG. 15. Extra particle stress around a disk in the presence of another disk as a function of the disk separation $\mathbf{r}(x,y)$ for $C \to 0$ (see Sec. IV). Extra particle stress is equal to 2 for a single disk.

### C. Semidilute suspensions

The effective viscosity of a semidilute suspension has been calculated for force-free spheres on several occasions [3,32]. Because the present problem is quite similar to the 3D case, we will only briefly discuss the main steps in the derivation and then provide the final answer. As shown in Ref. [49], the effective viscosity of a suspension of force-free particles can be calculated as

$$\eta = \eta_0 + \frac{1}{S\dot{\gamma}} \sum_{\alpha} \int_{\Gamma_\alpha} f_x y \, ds = \eta_0 - \frac{4\pi\eta_0}{S\dot{\gamma}} \sum_{\alpha} \Im A_1(\alpha), \tag{39}$$

where $\alpha$ indexes all particles, $\Gamma_\alpha$ is the contour of the particle $\alpha$, and $\boldsymbol{f}\,ds$ is the sum of forces acting from the infinitesimal arc of length $ds$ on the particle boundary. This force acts both on the fluid surrounding the particle, creating the flow disturbance, and inside the particle, in a way that cancels the imposed shear flow and the flow due to the other particles. The second equality in Eq. (39) is easy to check for circular objects considered here, but its validity is independent of particle shapes. The value $A_1$ for a given particle depends, generally speaking, on the states and relative positions of all other particles. Therefore, an averaging of some form is required to obtain a closed-form solution. Inasmuch as we are interested in the $\phi^2$ coefficient of the viscosity expansion in powers of the concentration $\phi$, only pairwise interactions of the disks have to be considered in our calculation. The main difficulty here is, however, that the integral of (38) over all possible relative orientations of the two disks does not converge absolutely [3,32]. We trace this difficulty to the fact that Eq. (38) was derived assuming that the distance $r$ between the disks be much smaller than the size of the region where the shear flow is imposed. Now if we allow the relative distance between two disks to go to infinity when averaging expression (38), this assumption will no longer be satisfied. We overcome this problem by first using the mean-field approximation, similarly to the method used in Ref. [3].

In the mean-field approximation, we consider a disk $D$ immersed in a dilute suspension of weakly interacting rigid disks. That is, (i) relative positions of the disks are not correlated and they can even overlap with each other and (ii) all disks have the same (but yet unknown) distribution of forces, which arise from the imposed flow and the hydrodynamic interaction with the other disks. Our plan

is to calculate the viscosity of a semidilute suspension of disks in the mean-field approximation and then to apply the corrections accounting for the fact that disks cannot overlap and for the properly calculated hydrodynamic interactions of two disks. In the mean-field approximation, each disk is suspended in a homogeneous effective medium that combines the hydrodynamic effects of both the solvent and the rigid disks. Applying shear rate $\dot{\gamma}$ to such a medium, results in a homogeneous distribution of viscous stress with an average value $\sigma_{xy}^{\mathrm{MF}} = \dot{\gamma}\eta_{\mathrm{MF}}$, where $\eta_{\mathrm{MF}}$ is the viscosity of the effective medium, which we can approximate by the viscosity of a dilute suspension of disks

$$\eta_{\mathrm{MF}} = \eta_0[1 + 2\phi + o(\phi)]. \tag{40}$$

Since the forces acting in the disk are proportional to the imposed viscous stress, we get the following expression for the effective viscosity of a semidilute suspension in the mean-field approximation $\eta_{\mathrm{MF}}$:

$$\eta_{\mathrm{MF}} = \eta_0[1 + 2\phi(1 + 2\phi) + o(\phi^2)]. \tag{41}$$

The first correction to expression (41) takes into account the fact that the disks cannot overlap. We calculate this correction in the following way: Given a disk $D$, we solve for the effective flow created by those disks $D_\alpha$ that overlap with it. The terms of $o(\phi^2)$ being neglected, this calculation can be performed with the simplification that the effects of all disks $D_\alpha$ can be taken independently of each other and of the disk $D$. Placing the origin of the coordinate plane at the center of the disk $D$ and denoting the center of the disk $D_\alpha$ by the complex number $\zeta_\alpha$, we observe that disk $D_\alpha$ creates the following distribution of force densities $\Phi(\zeta) = f_x(\zeta) + if_y(\zeta)$:

$$\Phi(\zeta) = 2i\dot{\gamma}\eta \int_0^{2\pi} \delta(\zeta - \zeta_\alpha - ae^{i\sigma})e^{-i\sigma} d\sigma. \tag{42}$$

The total force density created by disks overlapping with $D$ results from integration of (42) multiplied by the probability density of finding a disk $D_\alpha$ centered at $\zeta_\alpha$ and overlapping with $D$. This probability density reduces to $\phi H(2a - |\zeta_\alpha|)/\pi a^2$ when the disks are independently and homogeneously distributed. Here $H$ is the Heaviside function. Performing the integration, the following density of effective forces is obtained:

$$\Phi^{\mathrm{ol}}(\zeta) = 4i\dot{\gamma}\eta\overline{\zeta} \begin{cases} 0 & \text{if } |\zeta| \leqslant a \\ \sqrt{1 - \frac{(3a^2 - |\zeta|^2)^2}{4a^2|\zeta|^2}} & \text{if } a < |\zeta| < 3a \\ 0 & \text{if } |\zeta| \geqslant 3a, \end{cases} \tag{43}$$

where $\Phi^{\mathrm{ol}} = f_x^{\mathrm{ol}} + if_y^{\mathrm{ol}}$ and $\boldsymbol{f}^{\mathrm{ol}}$ is the effective force density created by all disks overlapping with the disk $D$. The flow disturbance produced by the forces (43) has a complicated form, but in the region occupied by the disk $D$, a simple straining flow is recovered:

$$\xi^{\mathrm{ol}}(\zeta) = i\dot{\gamma}\frac{\overline{\zeta}}{2} \quad \text{if } |\zeta| \leqslant a. \tag{44}$$

Equation (44) suggests that the disks overlapping with $D$ would create an additional strain rate $\dot{\gamma}\phi^2$ acting inside the disk $D$, which gives a contribution $2\phi^2\eta_0 + o(\phi^2)$ to the effective viscosity (41). Subtracting this contribution, we obtain

$$\eta_{\mathrm{no}} = \eta_0[1 + 2\phi(1 + \phi)] + o(\phi^2) \tag{45}$$

for the effective viscosity $\eta_{\mathrm{no}}$ of suspension of nonoverlapping noninteracting disks. The following intuitive explanation can be given for the expression (45): The average of the rate of strain $\partial_x u_y + \partial_y u_x$ in a suspension subjected to a shear rate $\dot{\gamma}$ is equal to $\dot{\gamma}$. This average can be decomposed into two contributions: The rate of strain inside the disks is equal to 0 and enters the average rate of strain in the whole suspension with the weight $\phi$. The average rate of strain inside the suspending fluid has weight $1 - \phi$ and therefore must be equal to $\dot{\gamma}/(1 - \phi) = \dot{\gamma}[1 + \phi + o(\phi)]$ for the average rate

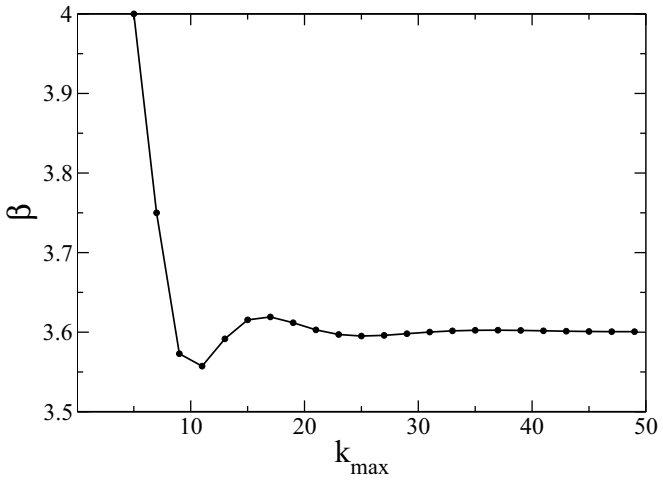


FIG. 16. Analytical result for the Batchelor coefficient $\beta$ of an unconfined suspension of rigid disks, shown as a function of $k_{\max}$, the order of truncation of the expansion of $\Im A_1$ in powers of $a/r$ [cf. Eq. (38)]. The results are shown only for even values of $k_{\max}$ because there are no odd powers in the expansion of $\Im A_1$. For $k_{\max} = 4$, $\beta \simeq 4$; for large $k_{\max}$ $\beta$ is close to 3.6.

of strain in the whole suspension to be equal to $\dot{\gamma}$. This means that each disk $D$ in the suspension is subject to an effective rate of strain equal to $\dot{\gamma}[1 + \phi + o(\phi)]$ due to the presence of the other disks if we neglect the effect of the presence of the disk $D$ on the distribution of velocities in the suspension. Because the coefficient $A_1$ in Eq. (39) is proportional to the rate of strain acting on the disk, we obtain the result (45).

The second correction must be applied to expression (45) in order to account for the short-range hydrodynamic interactions between the disks. Indeed, expression (45) was calculated with the simplification that when calculating the hydrodynamic effect of a disk $D_1$ on a disk $D_2$, the state of $D_1$ is taken as if no other disks, including $D_2$, were present. This effectively corresponds to neglecting all terms of $o((a/r)^2)$ in expression (38). Calculating the contribution of these terms to the effective viscosity of the semidilute suspension requires averaging all but the first two terms on the right-hand side of expression (37) over all possible relative positions of the two disks:

$$\eta_{\text{eff}} = \eta_{\text{no}} - \frac{4\phi^2}{\pi a^2 \dot{\gamma}} \int_0^{2\pi} d\theta \int_{2a}^{\infty} r\, dr\, \delta\Im A_1^{\text{pw}}(r,\theta), \tag{46}$$

where $\delta\Im A_1(r,\theta)$ is the correction to the value of $\Im A_1$,

$$\delta\Im A_1 = \Im A_1^{\text{pw}} - \dot{\gamma}\left(-\frac{a^2}{2} - \frac{a^4 \cos 4\theta}{r^2}\right). \tag{47}$$

The integral (46) converges absolutely due to the fact that the leading terms in Eq. (38) were split off and averaged during the calculation of $\eta_{\text{no}}$ in Eq. (45). This allows us to perform the integration (46) for a given number of terms in the expansion (38). Taking the $a^6/r^4$ term in Eq. (38) yields $\eta_{\text{eff}} = \eta_{\text{no}} + 2\eta_0\phi^2 + o(\phi^2) \approx \eta_0(1 + 2\phi + 4\phi^2)$, which coincides with the result reported in Ref. [37], where the same truncation of (38) was performed. Averaging further terms in Eq. (38) results in a slightly lower value of the Batchelor coefficient $\beta$. Truncating the expansion of $A_1^{\text{pw}}$ at the term $(a/r)^{64}$ gives us $\beta \approx 3.6$. The result of integration (46) is plotted as a function of $k_{\max}$, the number of terms taken in the expansion (38), in Fig. 16. The convergence is rather slow because of the nonanalytical behavior of $A_1^{\text{pw}}$ at $r = 2a$, which corresponds to the case when the two disks touch each other.

## V. CONCLUSION

In this paper we calculate the Einstein viscosity $[\eta]$ and the contribution of hydrodynamic interactions $\beta$ to the effective viscosity of a confined 2D suspension. For the less confined case ($C = 0.01$) we obtain the values $[\eta] = 2.0$ and $\beta = 3.6 \pm 0.1$, which are very close to the analytical values for an infinite fluid, i.e., $[\eta]_\infty = 2$ [36] and $\beta_\infty = 3.6$. Even for a nonconfined suspension the value $\beta_\infty = 3.6$ is not referenced in the literature. We show that the confined 3D suspension rheology can be clarified with the help of 2D simulations. The visualization of the entire flow in two dimensions combined with the calculation of dissipation allows us to understand why Einstein viscosity $[\eta]$ increases with the confinement: Regions of fluid squeezed between particles and walls have a high dissipation density. Our simulations also explain why the HI contribution of pairs of particles to the effective viscosity decreases with confinement and becomes negative: Dips of dissipation are created between close particles aligned along the shear flow. This effect is caused by the slowdown of angular velocity of close particles aligned along the flow. The confinement helps to force the particles into that specific configuration but similar results are obtained for nonconfined but aligned particles. Three-dimensional simulations confirm the interpretation deduced from the 2D results. If 2D models cannot of course replace 3D ones, we believe that the combination of both approaches can help to clarify some specific points at least qualitatively. Two-dimensional simulations are usually faster and are easier to implement and very convenient for data visualization. They can serve as a very efficient tool for the development of 3D simulations and for their understanding, but are also an important tool to understand hydrodynamic interactions between bioentities such as rafts and proteins [6] generally embedded in fluid biomembranes and which interact through 2D hydrodynamics.

## ACKNOWLEDGMENTS

This work was supported by the LabEx Tec 21 (Investissements d'Avenir Grant No. ANR-11-LABX-0030) and the ANR project Vivabrain (Grant No. ANR-12-MONU-0010). Most of the computations presented in this paper were performed using the Froggy platform of the CIMENT infrastructure [50], which is supported by the Rhône-Alpes region (Grant No. CPER07_13 CIRA) and the EquipMeso project (Grant No. ANR-10-EQPX-29-01). A.F. acknowledges financial support from Centre National d'Etudes Spatiales and European Space Agency.

## APPENDIX: DISK NEAR A FLAT WALL

The solution of the problem of two interacting disks can be easily modified to solve the problem of a disk near a flat wall. We place the wall at position $\Im\zeta = 0$ of the complex plane and denote the center of the disk as the complex number $\zeta_0 = iah_0$, where $ah_0$ is the distance of the center of the disk from the wall, as defined above. The velocity field $\xi = u_x + iu_y$ can be written in the form

$$\begin{aligned}\xi(\zeta) = {} & A(\zeta - \zeta_0) - (\zeta - \overline{\zeta})\overline{A'(\zeta - \zeta_0)} - A(\overline{\zeta} - \zeta_0) \\ & + B(\overline{\zeta} - \overline{\zeta}_0) - B(\zeta - \overline{\zeta}_0) + (\zeta - \overline{\zeta})\overline{B'(\zeta - \overline{\zeta}_0)},\end{aligned} \tag{A1}$$

which automatically satisfies the Stokes equation and the no slip boundary condition at the wall. The ansatz (A1) is a two-dimensional adaptation [51] of the Blake solution [52] recast in the complex form. The functions $A$ and $B$ can be represented as Laurent series about point $\zeta_0$, the coefficients of which can be found according to the scheme outlined in Sec. IV. The following result is then obtained:

$$[\eta]_{1\,\text{wall}} = 2 + \frac{2}{h_0^2} - \frac{1}{4h_0^4} + \frac{15}{16h_0^6} - \frac{49}{128h_0^8} + \frac{47}{128h_0^{10}} + \frac{35}{512h_0^{12}} + o\big(1/h_0^{12}\big). \tag{A2}$$

The convergence of the expansion (A2) is presented in Fig. 17.

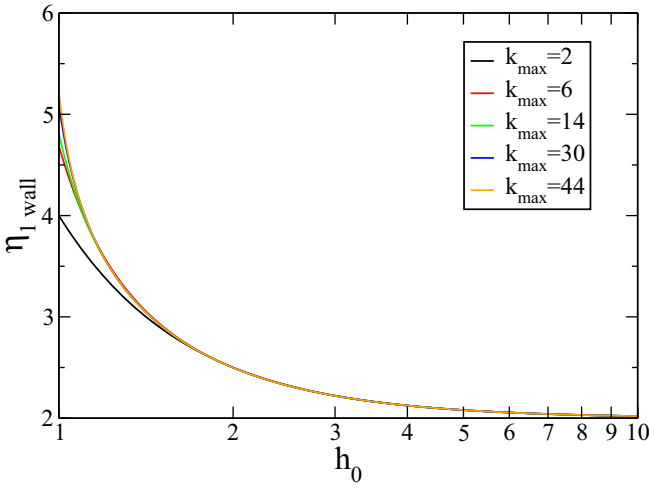


FIG. 17. Convergence of the analytical expression for the Einstein viscosity contribution $[\eta]_{1\,\mathrm{wall}}$ of a disk near a rigid wall, shown as a function of $h_0$ for several values of $k_{\max}$, the order of truncation of the expansion of $[\eta]_{1\,\mathrm{wall}}$ in powers of $1/h_0$ [Eq. (A2)].


[1] N. A. Frankel and A. Acrivos, On the viscosity of a concentrated suspension of solid spheres, Chem. Eng. Sci. **22**, 847 (1967).

[2] E. Guazzelli and J. Morris, *A Physical Introduction to Suspension Dynamics* (Cambridge University Press, Cambridge, 2012).

[3] S. Kim and S. J. Karilla, *Microhydrodynamics: Principles and Selected Applications* (Butterworths, Oxford, 1989).

[4] S. H. Lee and L. G. Leal, Low-Reynolds-number flow past cylindrical bodies of arbitrary cross-sectional shape, J. Fluid Mech. **164**, 401 (1986).

[5] C. R. Robertson and A. Acrivos, Low Reynolds number shear flow past a rotating circular cylinder. Part 1. Momentum transfer, J. Fluid Mech. **40**, 685 (1970).

[6] T. L. Dodd, D. A. Hammer, A. S. Sangani, and D. L. Koch, Numerical simulations of the effect of hydrodynamic interactions on diffusivities of integral membrane proteins, J. Fluid Mech. **293**, 147 (1995).

[7] M. Thiebaud, Z. Shen, J. Harting, and C. Misbah, Prediction of Anomalous Blood Viscosity in Confined Shear Flow, Phys. Rev. Lett. **112**, 238304 (2014).

[8] G. Ghigliotti, T. Biben, and C. Misbah, Rheology of a dilute two-dimensional suspension of vesicles, J. Fluid Mech. **653**, 489 (2010).

[9] P. R. Rao, G. I. Zahalak, and S. P. Sutera, Large deformations of elastic cylindrical capsules in shear flows, J. Fluid Mech. **270**, 73 (1994).

[10] H. C. Woolfenden and M. G. Blyth, Motion of a two-dimensional elastic capsule in a branching channel flow, J. Fluid Mech. **669**, 3 (2011).

[11] C. K. Aidun and Y. Lu, Lattice Boltzmann simulation of solid particles suspended in fluid, J. Stat. Phys. **81**, 49 (1995).

[12] J. Kromkamp, D. van den Ende, D. Kandhai, R. van der Sman, and R. Boom, Lattice Boltzmann simulation of 2D and 3D non-Brownian suspensions in Couette flow, Chem. Eng. Sci. **61**, 858 (2006).

[13] B. Cui, H. Diamant, B. Lin, and S. A. Rice, Anomalous Hydrodynamic Interaction in a Quasi-Two-Dimensional Suspension, Phys. Rev. Lett. **92**, 258301 (2004).

[14] S. Bhattacharya, J. Blawzdziewicz, and E. Wajnryb, Hydrodynamic interactions of spherical particles in suspensions confined between two plane walls, J. Fluid Mech. **541**, 263 (2005).

[15] S. Bhattacharya, J. Blawzdziewicz, and E. Wajnryb, Hydrodynamic interactions of spherical particles in Poiseuille flow between two parallel walls, Phys. Fluids **18**, 053301 (2006).
[16] M. E. Staben, A. Z. Zinchenko, and R. H. Davis, Motion of a particle between two parallel walls in low-Reynolds-number Poiseuille flow, Phys. Fluids **15**, 1711 (2011).
[17] J. W. Swan and J. F. Brady, Particle motion between parallel walls: Hydrodynamics and simulation, Phys. Fluids **22**, 103301 (2010).
[18] J. W. Swan and J. F. Brady, Anisotropic diffusion in confined colloidal dispersions: The evanescent diffusivity, J. Chem. Phys. **135**, 014701 (2011).
[19] Y. Davit and P. Peyla, Intriguing viscosity effects in confined suspensions: A numerical study, Europhys. Lett. **83**, 64001 (2008).
[20] P. Peyla and C. Verdier, New confinement effects on the viscosity of suspensions, Europhys. Lett. **94**, 44001 (2011).
[21] A. S. Sangani, A. Acrivos, and P. Peyla, Roles of particle-wall and particle-particle interactions in highly confined suspensions of spherical particles at low Reynolds numbers, Phys. Fluids **23**, 083302 (2011).
[22] M. Brust, O. Aouane, M. Thiebaud, D. Flormann, C. Verdier, L. Kaestner, M. W. Laschke, H. Selmi, A. Benyoussef, T. Podgorski, G. Coupier, C. Misbah, and C. Wagner, The plasma protein fibrinogen stabilizes clusters of red blood cells in microcapillary flows, Sci. Rep. **4**, 4348 (2014).
[23] M. K. Lyon and L. G. Leal, An experimental study of the motion of concentrated suspensions in two-dimensional channel flow, J. Fluid Mech. **363**, 25 (1998).
[24] P. R. Nott and J. F. Brady, Pressure-driven suspension flow: Simulation and theory, J. Fluid Mech. **275**, 157 (1994).
[25] H. Ez-Zahraouy, H. Mansouri, A. Benyoussef, P. Peyla, and C. Misbah, Rheology of a suspension of long plates in a poiseuille flow, Europhys. Lett. **79**, 54002 (2007).
[26] Y. Davit, J. M. Osborne, H. M. Byrne, D. Gavaghan, and J. Pitt-Francis, Validity of the Cauchy-Born rule applied to discrete cellular-scale models of biological tissues, Phys. Rev. E **87**, 042724 (2013).
[27] P. Tabeling, *Introduction to Microfluidics* (Oxford University Press, Oxford, 2005).
[28] W. Fornari, L. Brandt, P. Chaudhuri, C. U. Lopez, D. Mitra, and F. Picano, Rheology of Confined Non-Brownian Suspensions, Phys. Rev. Lett. **116**, 018301 (2016).
[29] I. M. Krieger and T. J. Dougherty, Dynamics of colloidal particles in soft matters, Trans. Soc. Rheol. **3**, 137 (1959).
[30] A. Einstein, Eine neue Bestimmung der Moleküldimensionen, Ann. Phys. (Leipzig) **19**, 289 (1906).
[31] A. Einstein, Berichtigung zu meiner Arbeit: "Eine neue Bestimmung der Moleküldimensionen", Ann. Phys. (Leipzig) **34**, 591 (1911).
[32] G. K. Batchelor and J. T. Green, The determination of the bulk stress in a suspension of spherical particles to order $c^2$, J. Fluid Mech. **56**, 401 (1972).
[33] B. Cichocki and B. U. Felderhof, Short-time diffusion coefficients and high frequency viscosity of dilute suspensions of spherical Brownian particles, J. Chem. Phys. **89**, 1049 (1988).
[34] H. S. Chen and A. Acrivos, The effective elastic moduli of composite materials containing spherical inclusions at non-dilute concentrations, Int. J. Solids Struct. **14**, 331 (1978).
[35] M. Belzons, R. Blanc, J.-L. Bouillot, and C. Camoin, Viscosité d'une suspension diluée et bidimensionnelle de sphères, C. R. Acad. Sci. Paris Série II **292**, 939 (1981).
[36] J. F. Brady, The Einstein viscosity correction in n dimensions, Int. J. Multiphase Flow **10**, 113 (1984).
[37] J. W. Ju and X. D. Zhang, Micromechanics and effective transverse elastic moduli of composites with randomly located aligned circular fibers, Int. J. Solids Struct. **35**, 941 (1998).
[38] J. Janela, A. Lefebvre, and B. Maury, A penalty method for the simulation of fluid - rigid body interaction, ESAIM: Proc. **14**, 201 (2005).
[39] A. Lefebvre, Fluid-particle simulations with FreeFem++, ESAIM: Proc. **18**, 120 (2007).
[40] H. Tanaka and T. Araki, Simulation Method of Colloidal Suspensions with Hydrodynamic Interactions: Fluid Particle Dynamics, Phys. Rev. Lett. **85**, 1338 (2000).
[41] P. Peyla, A deformable object in a microfluidic configuration: A numerical study, Europhys. Lett. **80**, 34001 (2007).

[42] B. Maury, Numerical analysis of a finite element/volume penalty method, SIAM J. Numer. Anal. **47**, 1126 (2009).
[43] L. Jibuti, S. Rafaï, and P. Peyla, Suspension with tunable effective viscosity. A numerical study, J. Fluid Mech. **693**, 345 (2012).
[44] V. Girault and P. A. Raviart, *Finite Element Methods for Navier-Stokes Equations: Theory and Algorithms* (Springer, Berlin, 1986).
[45] V. Doyeux, T. Podgorski, S. Peponas, M. Ismail, and G. Coupier, Spheres in the vicinity of a bifurcation: Elucidating the Zweifach-Fung effect, J. Fluid Mech. **674**, 359 (2011).
[46] F. Hecht, New development in FreeFem++, J. Numer. Math. **20**, 251 (2012); see also http://www.freefem.org/ff++
[47] J. Happel and H. Brenner, *Low Reynolds Number Hydrodynamics* (Nijhof, The Hague, 1983).
[48] A. Shapere and F. Wilczek, Self-Propulsion at Low Reynolds Number, Phys. Rev. Lett. **58**, 2051 (1987).
[49] G. K. Batchelor, The stress system in a suspension of force-free particles, J. Fluid Mech. **41**, 545 (1970).
[50] https://ciment.ujf-grenoble.fr
[51] C. Pozrikidis, *Boundary Integral and Singularity Methods for Linearized Viscous Flow* (Cambridge University Press, Cambridge, 1992).
[52] J. R. Blake, A spherical envelope approach to ciliary propulsion, J. Fluid Mech. **46**, 199 (1971).